JACS
JOURNAL OF THE AMERICAN CHEMICAL SOCIETY
Article
pubs.acs.org/JACS

Pt/In_2S_3/CdS/Cu_2ZnSnS_4 Thin Film as an Efficient and Stable Photocathode for Water Reduction under Sunlight Radiation

Feng Jiang,[†] Gunawan,[†] Takashi Harada,[†] Yongbo Kuang,[‡] Tsutomu Minegishi,[‡] Kazunari Domen,[‡] and Shigeru Ikeda*[,†]

[†]Research Center for Solar Energy Chemistry, Osaka University, 1-3 Machikaneyama, Toyonaka, Osaka 560-8531, Japan

[‡]Department of Chemical System Engineering, School of Engineering, The University of Tokyo, 7-3-1 Hongo, Bunkyo-ku, Tokyo 113-8656, Japan

Supporting Information

ABSTRACT: An electrodeposited Cu_2ZnSnS_4 (CZTS) compact thin film modified with an In_2S_3/CdS double layer and Pt deposits (Pt/In_2S_3/CdS/CZTS) was used as a photocathode for water splitting of hydrogen production under simulated sunlight (AM 1.5G) radiation. Compared to platinized electrodes based on a bare CZTS film (Pt/CZTS) and a CZTS film modified with a CdS single layer (Pt/CdS/CZTS), the Pt/In_2S_3/CdS/CZTS electrode exhibited a significantly high cathodic photocurrent. Moreover, the coverage of the In_2S_3 layer was found to be effective for stabilization against degradation induced by photocorrosion of the CdS layer. Bias-free water splitting with a power conversion efficiency of 0.28% was achieved by using a simple two-electrode cell consisting of the Pt/In_2S_3/CdS/CZTS photocathode and a $BiVO_4$ photoanode.

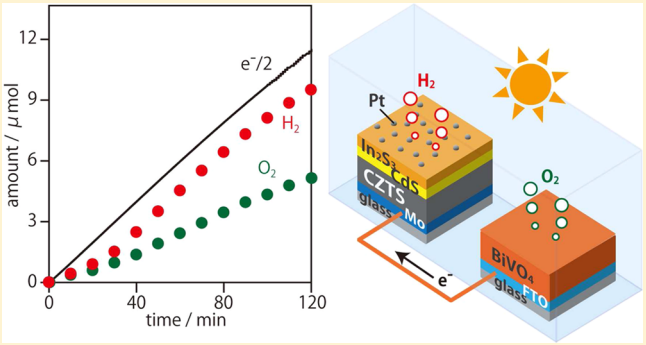

INTRODUCTION

Solar water splitting for production of hydrogen energy has attracted much attention due to its environmental friendliness and cost-effective property. Utilization of inorganic semiconductor thin films in photoelectrochemical (PEC) water splitting is an ideal approach to yield highly pure hydrogen energy. Various semiconductors used for solar cells, such as silicon,[1,2] III−V,[3−5] and I−II−VI,[6−15] have been studied for application in PEC hydrogen production because of their high absorption efficiency of the sunlight spectrum.

The Cu_2ZnSnS_4 (CZTS) compound is a promising absorber material for the next-generation photovoltaic thin-film module.[16−24] Due to its p-type semiconductive characteristics and optimum band gap for sunlight absorption (1.5 eV), the compound should also be promising as a photocathode for PEC water splitting. As the first example of a CZTS-based photocathode, Yokoyama et al. reported that an appreciably positive photocurrent onset potential of 0.7 V vs RHE (V_{RHE}; RHE = reversible hydrogen electrode) was obtained by modifications of a CdS layer and a TiO_2 compound followed by deposition of Pt particles.[25] Effects of the coatings of oxide layers on durability were also studied by Rovelli and Guijarro et al.[26,27] Wang and Ma et al. demonstrated that the use of Mo mesh as a back contact of the CZTS film modified with a CdS layer and Pt deposits resulted in an efficient photocurrent for hydrogen production under visible-light irradiation.[28,29] A porous CZTS film and a nanosheet-structured CZTS film were also employed as photocathodes for hydrogen production.[30,31] Moreover, nanocrystalline CZTS thin films were also investigated by several groups.[32,33] Although other examples have also been reported for water reduction over nanostructured CZTS electrode systems as well as particulate CZTS (i.e., photocatalytic) systems,[34,35] sacrificial electron donors were employed for hydrogen production in these studies. Hence, there are only four examples that discuss actual PEC water splitting over a CZTS-based photocathode as mentioned above.

One of the critical problems of PEC water splitting using a semiconductor photocathode is degradation and/or corrosion of the photocathode used; that is, appreciable reduction of the photocurrent (H_2 production) was usually observed during photoirradiation.[36] Regarding CZTS-based PEC water splitting, the stability issue has been discussed in only one report, but the electrode used in that study had a poor photocurrent.[26]

Recently, we found that the chemically deposited In_2S_3 buffer efficiently worked as a good buffer layer for a $CuInS_2$-based photocathode.[11,15] Moreover, a In_2S_3/CdS hybrid buffer was applied for a $Cu_2ZnSnSe_4$-based photovoltaic (PV) system: it gave PV performances comparable to those of the conventional CdS buffer.[37] These previous results and literature works motivated us to apply the In_2S_3 compound for the photocathode system. In this study, therefore, we employed a novel In_2S_3/CdS double layer for coverage of the CZTS film. When

Received: August 25, 2015
Published: October 8, 2015

DOI: 10.1021/jacs.5b09015
J. Am. Chem. Soc. 2015, 137, 13691−13697

conventional Pt catalyst particles were added to the In_2S_3/CdS/CZTS hybrid film, the thus-obtained photocathode showed a significant enhancement of stability during photoirradiation for PEC water splitting. The novel surface modification also resulted in a record half-cell solar to hydrogen efficiency (HC-STH) of 1.63% for a CZTS-based photocathode. Application of the efficient photocathode for bias-free water splitting by using a $BiVO_4$ counter photocathode was also demonstrated.

EXPERIMENTAL DETAILS

Preparation of CZTS Films. A CZTS thin film was prepared by electrodeposition of Cu, Sn, and Zn layers followed by sulfurization. Electrodeposition was carried out by using a Hokuto Denko HSV-100 potentiostat−galvanostat without stirring. A vertical three-electrode setup consisting of a Ag/AgCl reference electrode, a Pt wire counter electrode, and a Mo-coated glass substrate (Mo/glass) as a working electrode was employed. The Cu layer was deposited at −0.4 V (vs Ag/AgCl) using an electroplating bath containing 0.05 mol dm^{-3} $CuSO_4 \cdot 5H_2O$, 0.02 mol dm^{-3} citric acid, and 0.04 mol dm^{-3} trisodium citrate. For Sn deposition, 0.05 mol dm^{-3} Sn(II) methanesulfonate, 1 mol dm^{-3} methanesulfonic acid, and 1 mol dm^{-3} Empigen BB detergent (*n*-dodecyl-*N*,*N*-dimethylglycine) were used; the potential was fixed at −0.54 V (vs Ag/AgCl). The Zn layer was deposited at −1.2 V (vs Ag/AgCl) using a bath solution containing $ZnSO_4 \cdot 7H_2O$ (0.1 mol dm^{-3}) and K_2SO_4 (0.5 mol dm^{-3}) with pH adjusted to 3 using a HYDRON buffer. The Cu/Zn/Sn stack as-deposited was then heated at 320 °C for 200 min in an evacuated Pyrex ampule, followed by sulfurization in the presence of 5−10 mg of elemental sulfur powder in an evacuated Pyrex ampule at 590 °C for 10 min.[22−24] Thus-obtained CZTS films were then treated in an aqueous KCN solution (10%) for 2 min to remove surface contaminants.

Surface Modification with n-Type Thin Layers. Surface modification of the prepared CZTS film by CdS and In_2S_3 layers was performed by the chemical bath deposition method. The prepared CZTS film was immersed in an aqueous solution containing 12.5 mmol dm^{-3} $CdSO_4$, 0.22 mol dm^{-3} $SC(NH_2)_2$, and 11 mol dm^{-3} NH_4OH at 60 °C for 7 min to yield CdS-covered CZTS (CdS/CZTS). The In_2S_3 layer was deposited onto the CdS/CZTS film by using a solution composed of 25 mol dm^{-3} $In_2(SO_4)_3$, 0.1 mol dm^{-3} CH_3CSNH_2, and 0.1 mol dm^{-3} CH_3COOH; the In_2S_3 deposition was performed at 65 °C for 15 min to form In_2S_3-covered CZTS (In_2S_3/CdS/CZTS).[11,13]

Surface Modification with Pt. Pt particles were deposited on CdS/CZTS and In_2S_3/CdS/CZTS films by photoelectrodeposition. The deposition was performed by using a three-electrode system consisting of CdS/CZTS or as a working electrode, a Pt wire as a counter electrode, and Ag/AgCl as a reference electrode. These electrodes were put in 0.1 M Na_2SO_4 solution containing 1 mM H_2PtCl_6, and the deposition was performed with a constant potential of −0.1 V for 10 min by using a Solartron SI1280B electrochemical measurement unit. During the deposition, the working electrode was illuminated by simulated AM 1.5G solar irradiation from an Asahi Spectra HAL320 solar simulator. The light intensity was calibrated by measuring a current−voltage (*J*−*V*) curve of a standard Si solar cell. Thus-obtained Pt-modified films were labeled Pt-CdS/CIGS and Pt-In_2S_3/CdS/CZTS.

PEC Measurements. The same three-electrode setup as that used for the Pt deposition (see above) was used for PEC measurements of photocathodes. PEC H_2 generation from photocathodes was examined in a pH 6.5 phosphate buffer solution (0.2 mol dm^{-3} Na_2HPO_4/NaH_2PO_4) by using the above-mentioned solar simulator as a light source. Potentials referred to the Ag/AgCl electrode were converted to reversible hydrogen electrode using the Nernst equation:

$$V_{RHE} = V_{Ag/AgCl} + 0.059 \times pH + 0.199$$

HC-STH was determined from the current density−potential response of the photocathodes by using the following equation:[15,38]

$$\text{HC-STH}\ (\%) = J \times V \times 100/P$$

where J is the photocurrent density (mA cm^{-2}), V is the applied potential (V_{RHE}), and P is the intensity of simulated sunlight (100 mW cm^{-2}).

A PEC cell connected to an online gas chromatography system (Agilent 490 Micro GC gas analyzer equipped with a MS-5A column and a thermal conductivity detector) was used to detect H_2 and O_2 during the PEC water splitting. The PEC cell was covered by a water jacket to maintain the temperature at 293 K. For the three-electrode setup, photoirradiation was performed at 0 and 0.5 V_{RHE} by using the solar simulator. The two-electrode setup composed of the Pt-In_2S_3/CdS/CZTS photocathode and a $BiVO_4$-based photoanode[39] in series connection was also employed to examine water splitting under the bias-free condition.

Structural Characterization. Crystalline structures of the films were determined by X-ray diffraction (XRD) using a Rigaku Mini Flex X-ray diffractometer (Cu Kα, Ni filter) and Raman spectroscopy using a Jasco NRC 3100 laser raman spectrophotometer. Morphologies of the films were examined using a Hitachi S-5000 FEG field emission scanning electron microscope (SEM) at an acceleration voltage of 20 kV. Elemental compositions of the films were determined using a Hitachi TM3000 SEM equipped with a SwiftED3000 energy-dispersive X-ray spectrometer (EDX). Surface and bulk chemical structures of photoelectrodes were examined by X-ray photoelectron spectroscopy (XPS) using a Shimadzu AXIS ULTRA X-ray photoelectron spectrometer.

RESULTS AND DISCUSSION

The CZTS film used in this study was prepared by sulfurization of electrodeposited Cu/Sn/Zn stacks on a Mo-coated glass substrate.[22−24] As confirmed by XRD and Raman spectroscopic analyses, the thus-obtained CZTS film was crystallized in a kesterite structure without other secondary phases (Figure S1). When compared to the stoichiometric composition, a relatively Cu-poor and Zn-rich composition (Cu/Zn/Sn/S = 23/14/13/50), which is suitable for showing a p-type characteristic, was confirmed by EDX analysis of the film. As shown in Figure 1a,b, surface and cross-sectional SEM images of the CZTS film indicated that well-grown crystallites with grain sizes of ca. 1.5 μm were densely packed on the substrate.

Surface modifications of the CZTS film with n-type compounds were performed by using the chemical bath deposition technique.[11,22−24] Figure 1c shows a surface SEM image of the CZTS film modified with a CdS layer. Compared

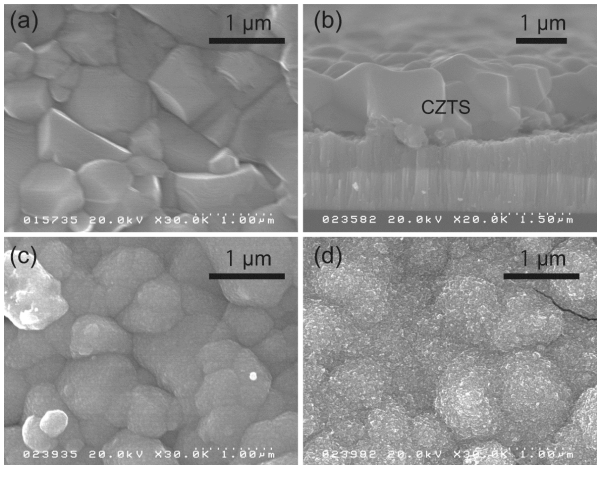

Figure 1. Surface (a) and cross-sectional (b) SEM images of CZTS and surface SEM images of CdS/CZTS (c) and In_2S_3/CdS/CZTS (d).

DOI: 10.1021/jacs.5b09015
J. Am. Chem. Soc. 2015, 137, 13691−13697

to the surface image of bare CZTS (Figure 1a), the surface morphology was appreciably changed: the surface of each CZTS grain was entirely covered with small CdS particles. After deposition of an In_2S_3 layer onto the CdS-covered CZTS, the appearance of the surface morphology was also changed from that before the In_2S_3 deposition. As shown in Figure 1d, the In_2S_3 layer not only covered the CdS/CZTS grains but also filled their grain boundaries, suggesting efficient protection without exposing the CdS component on the In_2S_3/CdS/CZTS stack. In addition, these chemically deposited CdS and In_2S_3 layers would be deposited as β-CdS and β-In_2S_3, respectively, as observed by weak diffractions of corresponding materials in XRD patterns and Raman spectra of these layers deposited on a glass substrate (Figure S2). As reported previously, the band gap energies (E_g) of CdS and In_2S_3 films were estimated to be 2.44 and 2.24 eV, respectively.[15]

Figure 2a shows typical current density−potential curves obtained by modified CZTS electrodes under chopped illumination of simulated sunlight (AM 1.5G). Because of the large hydrogen overpotential of the bare CZTS film, deposition of Pt was required to enhance the surface reaction rate; however, the observed photocurrent of the Pt-modified CZTS (Pt-CZTS) film was not significant. Appreciable enhancement of the photocurrent was achieved by modification with a chemical-bath-deposited CdS layer between the CZTS film and Pt deposits to form a Pt/CdS/CZTS structure, as expected from similar systems reported in the literature.[25−28] Photocurrent density at 0 V_{RHE} and photocurrent onset potential of the present Pt/CdS/CZTS electrode at pH 6.5 reached −4.5 mA cm^{-2} and 0.62 V_{RHE}, respectively. The appreciable improvement in photocathodic properties should be caused by enhancement of spatial charge separation due to the formation of a p−n junction between the CZTS film and the CdS layer.

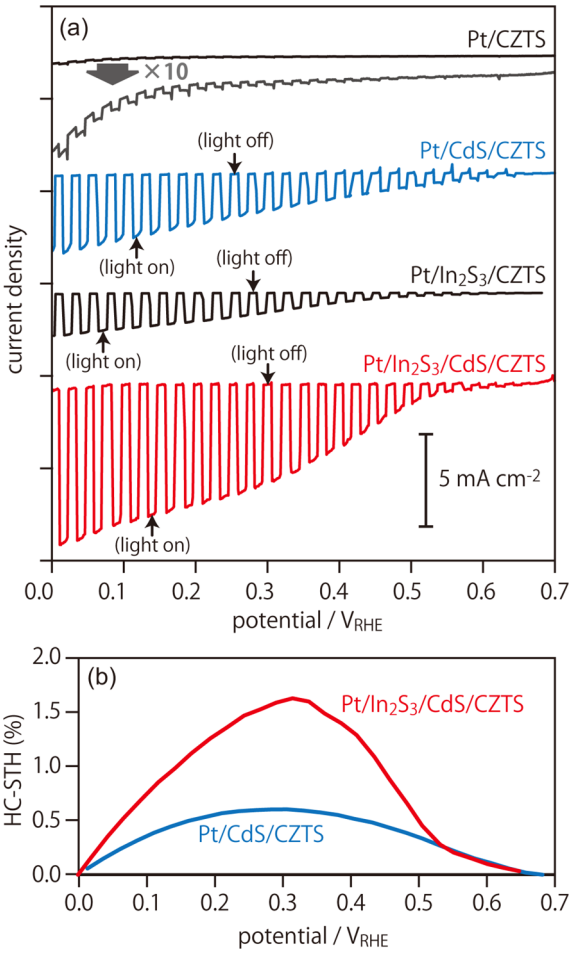

Figure 2. Current density−potential curves of Pt/CZTS, Pt/CdS/CZTS, and Pt/In_2S_3/CdS/CZTS photocathodes in a 0.2 mol dm^{-3} Na_2HPO_4/NaH_2PO_4 solution (pH 6.5) under chopped solar-simulated AM 1.5G light irradiation (a) and corresponding HC-STH efficiency curves of Pt/CdS/CZTS and Pt/In_2S_3/CdS/CZTS photocathodes (b).

When the In_2S_3 buffer was used instead of CdS, the thus-obtained Pt/In_2S_3/CZTS photocathode did not work well compared to the Pt/CdS/CZTS electrode, probably due to a junction property of the In_2S_3−CZTS interface that is worse than that of the CdS−CZTS interface. On the other hand, the use of an In_2S_3/CdS double layer instead of a CdS single layer (i.e., use of the Pt/In_2S_3/CdS/CZTS electrode) appreciably enhanced current density: the photocurrent of the Pt/In_2S_3/CdS/CZTS electrode reached −9.3 mA cm^{-2} at 0 V_{RHE}, though its onset potential of 0.63 V_{RHE} is almost the same as that of the Pt/CdS/CZTS electrode. Calculation of the solar conversion efficiency in HC-STH using current density−potential curves showed that the highest HC-STH of the present Pt/In_2S_3/CdS/CZTS electrode reached 1.63%, which is a record value for a CZTS-based photoelectrode, at 0.31 V_{RHE}, whereas that of Pt/CdS/CZTS was ca. 0.61% at 0.28 V_{RHE}, as shown in Figure 2b. The observation of a relatively steep rise of photocurrent at the onset region on the Pt/In_2S_3/CdS/CZTS electrode when compared to that on the Pt/CdS/CZTS electrode, leading to an appreciable enhancement of the current density in the entire potential range from onset potential to highly negative potential, implies reduction of series resistance induced by introduction of the In_2S_3 interlayer. Hence, the In_2S_3 layer in the Pt/In_2S_3/CdS/CZTS electrode should have sufficient conductivity and favorable electronic contacts to both the CdS layer and Pt deposits. This modification is likely to provide an electronic contact at the Pt/In_2S_3 interface better than that of the Pt/CdS interface. Appreciable degradation of the Pt/CdS/CZTS electrode is another possible explanation for the difference in photocurrents (see below). It should also be noted that diffusion of In from In_2S_3 into CdS and $Cu_2ZnSn(S,Se)_4$ has been reported in a photovoltaic system; this would induce n-type doping in CdS and p-type doping in $Cu_2ZnSn(S,Se)_4$ to enhance carrier concentrations of both buffer and absorber layers.[37] However, the fact that photocurrent onset potentials between Pt/In_2S_3/CdS/CZTS and Pt/CdS/CZTS electrodes were almost constant suggests no occurrence of compositional and structural modification at the CdS/CZTS interface by surface coverage of the In_2S_3 layer in the present system. Such improvements of photocurrent onset potentials would be achieved by addition of appropriate heat treatments to induce In diffusion.

Incident photon to current efficiency (IPCE) of the Pt/In_2S_3/CdS/CZTS electrode was measured under irradiation of monochromatic light with various wavelength at 0 V_{RHE}. The obtained IPCE spectrum is shown in Figure S3a. The spectrum showed IPCE of 45−50% at wavelengths ranging from ca. 400 to 700 nm; the IPCE value declined steeply at wavelengths longer than 700 nm. By applying the deformation of the spectra into $[h\nu\ \ln(1 - \mathrm{IPCE})]^2$ versus photon energy ($h\nu$/eV) plot at the onset region, the band gap energy (E_g) of the CZTS film

DOI: 10.1021/jacs.5b09015
J. Am. Chem. Soc. 2015, 137, 13691−13697

under the Pt/In_2S_3/CdS stacked modifier was estimated to be 1.45 eV (Figure S3b).

Most of photocathode compounds have shown a degradation problem. Our continual studies on the CdS-modified $CuInS_2$ system also showed such a problem[11] with the exception of very recent results.[12] Hence, stabilities of the present electrode systems were studied by measuring time-dependent photocurrent profiles at 0 V_{RHE}. Results for Pt/CdS/CZTS and Pt/In_2S_3/CdS/CZTS electrodes are shown in Figure 3. An obvious

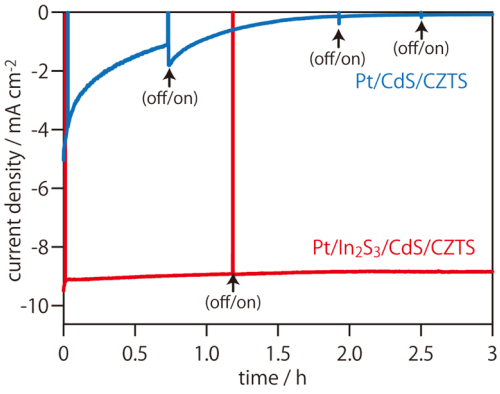

Figure 3. Current−time curves for Pt/CdS/CZTS and Pt/In_2S_3/CdS/CZTS electrodes in 0.2 mol dm^{-3} Na_2HPO_4/NaH_2PO_4 solution (pH 6.5) at 0 V_{RHE} under photoirradiation from simulated sunlight (AM 1.5G).

photocurrent decay was observed for the Pt/CdS/CZTS electrode: photocurrent density had decreased to −0.08 mA cm^{-2} after a 3 h durability test, even though an appreciable photocurrent was observed at the initial stage. Compared to the Pt/CdS/CZTS electrode, the Pt/In_2S_3/CdS/CZTS electrode exhibited good properties: it gave a significantly high photocurrent without showing an appreciable decrease after the 3 h reaction. Relatively high current density of the electrode compared to that of the Pt/CdS/CZTS electrode observed in the above current density−potential curves (see Figure 2a) was, therefore, partly due to the rapid photocurrent drop observed for the Pt/CdS/CZTS electrode without the In_2S_3 layer.

Figure 4 shows cross-sectional SEM images of Pt/CdS/CZTS and Pt/In_2S_3/CdS/CZTS samples before and after the 3 h durability test. The original Pt/CdS/CZTS photocathode showed a homogeneous coverage of a dense 150 nm thick CdS layer that forms a CdS/CZTS-layered structure, as shown in Figure 4a. The Pt/In_2S_3/CdS/CZTS showed a relatively thick overlayer of In_2S_3/CdS stack of ca. 300 nm thickness (Figure 4c). The stacked structure of the In_2S_3/CdS double layer was confirmed by a depth profile analysis of the Pt/In_2S_3/CdS/CZTS sample using XPS (details are given in Supporting Information, Figure S4). It should be noted that there are almost no distinguishable Pt particles in the SEM image of both Pt/CdS/CZTS and Pt/In_2S_3/CdS/CZTS samples, owing to small loading amounts. However, the presence of metallic Pt components on the electrode after photodeposition was confirmed by XPS analyses.

After the durability test, the Pt/CdS/CZTS sample showed considerable change in the CdS layer; that is, nondense and granular particles were dispersed on the surface of the CZTS film (Figure 4b). Since an obvious change in the ratio of spectral intensities of CdS (1LO mode) and CZTS (A1 mode) peaks was observed in the Raman spectra of the Pt/CdS/CZTS

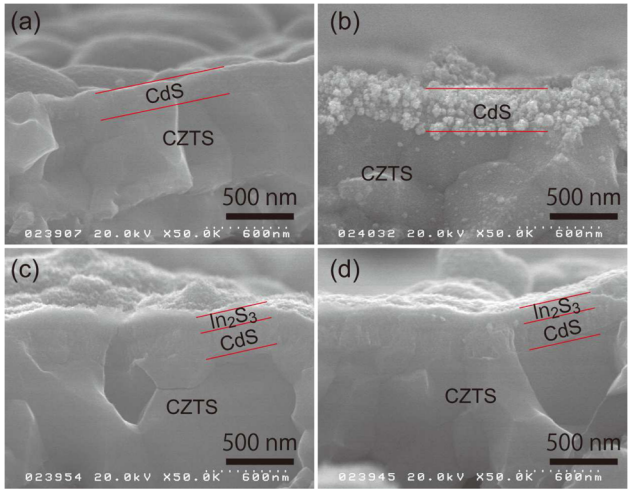

Figure 4. Cross-sectional SEM images of Pt/CdS/CZTS (a,b) and Pt/In_2S_3/CdS/CZTS (c,d) photocathodes before (a,c) and after (b,d) a 3 h durability test.

sample after the durability test (Figure S5a), partial dissolution of the CdS layer should occur during the PEC reaction. In contrast, the morphology and structure of the In_2S_3/CdS double layer was almost constant before and after the reaction, as shown in Figure 4c,d. No obvious change in the intensity ratio of CdS (1LO mode) and CZTS (A1 mode) Raman peaks (Figure S6) also indicates that much less damage of the In_2S_3/CdS double layer was induced by the PEC reaction.

Based on the fact that a stable, but an appreciably low (<0.1 mA cm^{-2}), photocurrent flow was observed on the Pt/CZTS electrode (data not shown), the observed low stability of the Pt/CdS/CZTS was likely to be derived from the instability of the CdS layer when it contacted an electrolyte under irradiation. Although the essential reason was not clarified yet, these results suggest that an appreciable decline of photocurrent on the Pt/CdS/CZTS was attributed to the specific photoreactivity of CdS.

The Cd 3d XP spectrum of the Pt/CdS/CZTS sample after the durability test showed the presence of appreciable shoulder components assignable to CdO[40] in addition to intense peaks derived from CdS, which were observed as a sole component in the XP spectrum of the original Pt/CdS/CZTS sample, as shown in Figure S5b. It is well-known that CdS in a photocatalytic system leads to oxidative self-photocorrosion by photogenerated positive holes.[41] Moreover, partial reduction of CdS to form zero-valent Cd^0 was also probable (the Cd^0 component, if present, should be oxidized spontaneously by exposure to open air before XP spectroscopic measurement).[42] Due to insufficient evidence in this study, we cannot draw a conclusion about the main corrosion pathway of the CdS layer at present. However, our results indicate that such corrosion reactions can be suppressed by coverage with an In_2S_3 layer to avoid direct contact of the CdS layer with an electrolyte. This facile strategy should be applicable to various photocathode systems for PEC water splitting.

The amounts of evolved H_2 from the Pt/In_2S_3/CdS/CZTS photocathode were measured in the three-electrode system at several potentials under AM 1.5G radiation. Figure 5 shows typical time course curves of H_2 evolution from the photocathode with an active surface area of 0.3 cm^2 and one-half of the electrons passing through the outer circuit ($e^-/2$). When the reaction was performed at 0 V_{RHE}, the amount of H_2

DOI: 10.1021/jacs.5b09015
J. Am. Chem. Soc. 2015, 137, 13691−13697

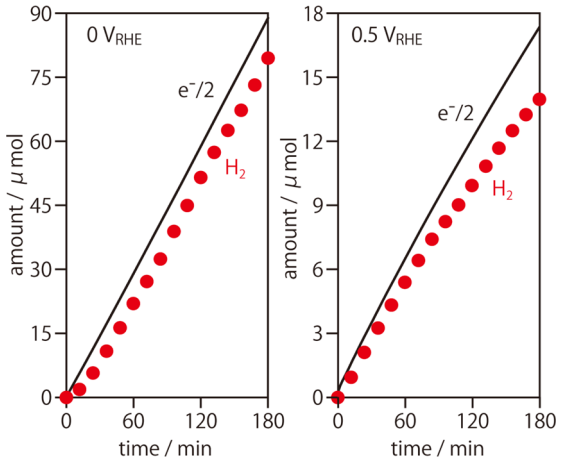

Figure 5. Time course curves of H_2 evolution over the $Pt/In_2S_3/CdS/CZTS$ photocathode in the conventional three-electrode configuration under simulated sunlight (AM 1.5G) radiation at 0 and 0.5 V_{RHE}. The solid lines denote time course curves of one-half of the electrons passing through the outer circuit ($e^-/2$).

monotonically accumulated at a constant rate of 0.477 μmol min^{-1} after a short (ca. 20 min) induction period. The presence of the induction period in the H_2 accumulation curve was likely to be due to the adhesion of generated H_2 in the initial stage. The total amount of evolved H_2 after 2 h photoirradiation (H_2: 52 μmol) was much larger than the molar amount of CZTS (less than 2 μmol on the 0.3 cm^{-2} device used), indicating catalytic function of the present system without any degradation. Faradaic efficiency determined from the ratio of the rate of H_2 evolution to that of $e^-/2$ (0.495 μmol min^{-1}) was close to unity (96%), indicating that there should be no other reduction/oxidation process. A monotonic H_2 accumulation was also confirmed by the PEC system operated at the potential close to the onset region (0.5 V_{RHE}). However, an appreciable decrease in H_2 evolution accompanied by a decrease in the rate of $e^-/2$ was observed. Estimated Faradaic efficiencies determined in the initial half period (0–90 min) and the latter half period (90–120 min) were 89 and 79%, respectively. These results suggest the occurrence of gradual degradation of the $Pt/In_2S_3/CdS/CZTS$ electrode. Decay of the photocurrent induced by operating the reaction in a relatively positive bias region (0.5 V_{RHE}) was also observed on the $Cu(In,Ga)Se_2$-based photocathode, the surface of which was modified with a CdS buffer layer followed deposition of a Ti and/or Mo protective layer and a Pt catalyst.[14] However, the present $Pt/In_2S_3/CdS/CZTS$ electrode seemed to be more robust to perform the reaction for several hours.

The above properties of the $Pt/In_2S_3/CdS/CZTS$ photocathode indicate sufficient applicability of the electrode to a two-electrode system for bias-free water splitting. For this purpose, a $BiVO_4$ film deposited on a fluorine-coated glass substrate (FTO/glass) was prepared for use as a counter photoanode for O_2 production.[39] Figure 6a shows a typical current–potential curve obtained by the $BiVO_4$ electrode with an active area of 0.50 cm^2. The curve of the $Pt/In_2S_3/CdS/CZTS$ photocathode used for this system having an active area of 0.63 cm^2 was also plotted by using absolute current values. An appreciable overlap between these anodic and cathodic photocurrents with an intersecting potential of 0.5 V_{RHE} was confirmed, indicating possible induction of water splitting. Indeed, a two-electrode system, such as two electrodes simply

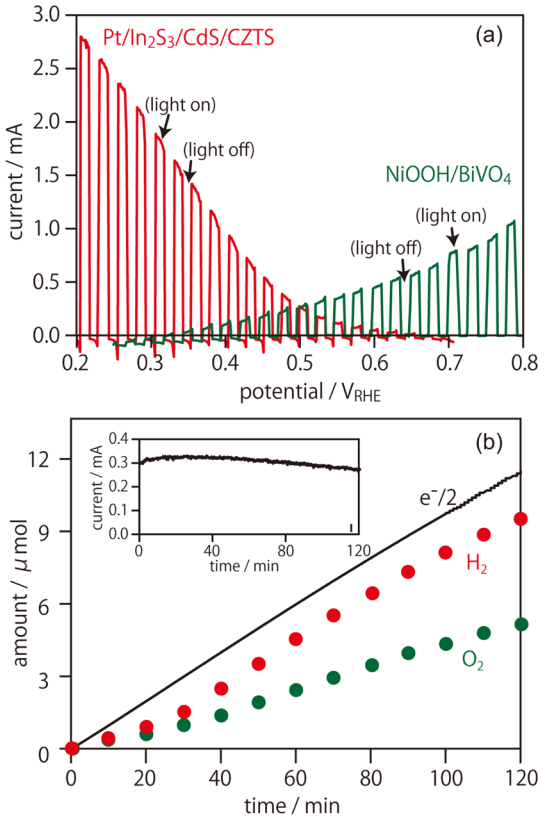

Figure 6. Current density–potential curves of $BiVO_4$ photoanode and $Pt/In_2S_3/CdS/CZTS$ photocathode in 0.2 mol dm^{-3} Na_2HPO_4/NaH_2PO_4 solution (pH 6.5) under chopped solar-simulated AM 1.5G light irradiation (a). Time course curves of H_2 and O_2 evolution over the $Pt/In_2S_3/CdS/CZTS$-$BiVO_4$ two-electrode cell under simulated sunlight (AM 1.5G) radiation. The solid line denotes the time course curve of $e^-/2$. Inset shows the corresponding net current–time curve.

connected through a conducting wire, could generate stoichiometric amounts of H_2 and O_2 under simulated sunlight (AM 1.5G) irradiation, as shown in Figure 6b. As expected from the intersecting potential between these two electrodes, the working potential of the present system should be highly positive. Hence, gradual degradation of the $Pt/In_2S_3/CdS/CZTS$ photocathode occurred, and thereby a gradual drop in both H_2 and O_2 accumulation as well as a decline in net photocurrents (inset in Figure 6b) was observed. Since the total active area of the two electrodes used was 1.13 cm^2, the sum of the energy irradiated to these electrodes for 2 h was estimated to be 0.799 kJ, corresponding to 3.37 mmol of H_2 production from the water splitting reaction. Based on the amount of H_2 accumulated for 2 h (9.5 μmol), power conversion efficiency (PCE) in the present system was estimated to be 0.28%. To the best of our knowledge, this is the first reported example of an appreciable occurrence of bias-free water splitting using a CZTS-based photocathode. As mentioned above, the stability of the $Pt/In_2S_3/CdS/CZTS$ photocathode as well as the efficiency of H_2 liberation should be improved when the operation potential becomes more negative. Hence, with the use of optimum photoanodes, which enable induction of water oxidation under relatively cathodic polarization, a robust and highly active water splitting system should be realized.

DOI: 10.1021/jacs.5b09015
J. Am. Chem. Soc. 2015, 137, 13691–13697

CONCLUSIONS

A compact CZTS thin film prepared by sulfurization of electrodeposited metallic stacks on a Mo-coated glass substrate was used as the base photocathode in this work. Modification with an In_2S_3/CdS double layer followed by deposition of particulate Pt catalysts resulted in induction of efficient PEC reduction of water with the maximum HC-STH of 1.63% without showing appreciable degradation. The In_2S_3 layer acts a mediator for efficient electron transport to Pt deposits as well as a protecting layer to avoid contact between the CdS layer and outer electrolyte solution. The Pt/In_2S_3/CdS/CZTS electrode was proven to work as the water reduction part of a two-electrode PEC solar water splitting module for the first time, though further systemic optimizations and further studies to enhance both durability and activity are necessary for considering future practical use.

ASSOCIATED CONTENT

Supporting Information

The Supporting Information is available free of charge on the ACS Publications website at DOI: 10.1021/jacs.5b09015.

XRD and Raman spectra of CZTS, CdS, and In_2S_3 films, IPCE spectra of the Pt/In_2S_3/CdS/CZTS photocathode, depth XP analyses of the In_2S_3/CdS/CZTS heterostructure, Raman and XP spectra of Pt/CdS/CZTS and Pt/In_2S_3/CdS/CZTS photocathodes before and after PEC water splitting (PDF)

AUTHOR INFORMATION

Corresponding Author

*sikeda@chem.es.osaka-u.ac.jp

Notes

The authors declare no competing financial interest.

ACKNOWLEDGMENTS

This work was carried out as part of a program supported by NEDO Japan. This work was also supported by a Grant-in-Aid for Scientific Research on Innovative Areas (All Nippon Artificial Photosynthesis Project for Living Earth) and a Grant-in-Aid for Scientific Research (B) from MEXT, Japan. Feng Jiang is acknowledged for a JSPS Postdoctoral Fellowship.

REFERENCES

(1) Hu, S.; Shaner, M. R.; Beardslee, J. A.; Lichterman, M.; Brunschwig, B. S.; Lewis, N. S. *Science* **2014**, *344*, 1005−1009.
(2) Oh, J.; Deutsch, T. G.; Yuan, H.; Branz, H. M. *Energy Environ. Sci.* **2011**, *4*, 1690−1694.
(3) Nakato, Y.; Tonomura, S.; Tsubomura, H. *Ber. Bunsenges. Phys. Chem.* **1976**, *80*, 1289−1293.
(4) Heller, A.; Aharon-Shalom, E.; Bonner, W. A.; Miller, B. *J. Am. Chem. Soc.* **1982**, *104*, 6942−6948.
(5) Khaselev, O.; Turner, J. A. *Science* **1998**, *280*, 425−427.
(6) Miller, E.; Paluselli, E.; Marsen, B.; Rocheleau, R. *Electrochem. Solid-State Lett.* **2005**, *8*, A247−A249.
(7) Kaneshiro, J.; Gaillard, N.; Rocheleau, R.; Miller, E. *Sol. Energy Mater. Sol. Cells* **2010**, *94*, 12−16.
(8) Ikeda, S.; Nakamura, T.; Lee, S. M.; Yagi, T.; Harada, T.; Minegishi, T.; Matsumura, M. *ChemSusChem* **2011**, *4*, 262−268.
(9) Moriya, M.; Minegishi, T.; Kumagai, H.; Katayama, M.; Kubota, J.; Domen, K. *J. Am. Chem. Soc.* **2013**, *135*, 3733−3735.
(10) Kumagai, H.; Minegishi, H.; Moriya, Y.; Kubota, J.; Domen, K. *J. Phys. Chem. C* **2014**, *118*, 16386−16392.
(11) Gunawan; Septina, W.; Ikeda, S.; Harada, T.; Minegishi, T.; Domen, K.; Matsumura, M. *Chem. Commun.* **2014**, *50*, 8941−8943.
(12) Zhao, J.; Minegishi, T.; Zhang, L.; Zhong, M.; Gunawan; Nakabayashi, M.; Ma, G.; Hisatomi, T.; Katayama, M.; Ikeda, S.; Shibata, N.; Yamada, T.; Domen, K. *Angew. Chem., Int. Ed.* **2014**, *53*, 11808−11812.
(13) Septina, W.; Gunawan; Ikeda, S.; Harada, T.; Higashi, M.; Abe, R.; Matsumura, M. *J. Phys. Chem. C* **2015**, *119*, 8576−8583.
(14) Kumagai, H.; Minegishi, T.; Sato, N.; Yamada, T.; Kubota, J.; Domen, K. *J. Mater. Chem. A* **2015**, *3*, 8300−8307.
(15) Gunawan; Septina, W.; Harada, T.; Nose, Y.; Ikeda, S. *ACS Appl. Mater. Interfaces* **2015**, *7*, 16086−16092.
(16) Cao, Y.; Denny, M. S., Jr.; Caspar, J. V.; Farneth, W. E.; Guo, Q.; Ionkin, A. S.; Johnson, L. K.; Lu, M.; Malajovich, I.; Radu, D.; Rosenfeld, H. D.; Choudhury, K. R.; Wu, W. *J. Am. Chem. Soc.* **2012**, *134*, 15644−15647.
(17) Siebentritt, S.; Schorr, S. *Prog. Photovoltaics* **2012**, *20*, 512−519.
(18) Todorov, T. K.; Tang, J.; Bag, S.; Gunawan, O.; Gokmen, T.; Zhu, Y.; Mitzi, D. B. *Adv. Energy. Mater.* **2013**, *3*, 34−38.
(19) Scragg, J. J.; Dale, P. J.; Peter, L. M.; Zoppi, G.; Forbes, I. *Phys. Status Solidi B* **2008**, *245*, 1772−1778.
(20) Guo, L.; Zhu, Y.; Gunawan, O.; Gokmen, T.; Deline, V. R.; Ahmed, S.; Romankiw, L. T.; Deligianni, H. *Prog. Photovoltaics* **2014**, *22*, 58−68.
(21) Ahmed, S.; Reuter, K. B.; Gunawan, O.; Guo, L.; Romankiw, L. T.; Deligianni, H. *Adv. Energy. Mater.* **2012**, *2*, 253−259.
(22) Lin, Y.; Ikeda, S.; Septina, W.; Harada, T.; Matsumura, M. *Sol. Energy Mater. Sol. Cells* **2014**, *120*, 218−225.
(23) Jiang, F.; Ikeda, S.; Harada, T.; Matsumura, M. *Adv. Energy Mater.* **2014**, *4*, 1301381.
(24) Jiang, F.; Ikeda, S.; Tang, Z.; Minemoto, T.; Septina, W.; Harada, T.; Matsumura, M. *Prog. Photovoltaics* **2015**, DOI: 10.1002/pip.2638.
(25) Yokoyama, D.; Minegishi, T.; Jimbo, K.; Hisatomi, T.; Ma, G.; Katayama, M.; Kubota, J.; Katagiri, H.; Domen, K. *Appl. Phys. Express* **2010**, *3*, 101202.
(26) Rovelli, L.; Tilley, S. D.; Sivula, K. *ACS Appl. Mater. Interfaces* **2013**, *5*, 8018−8014.
(27) Guijarro, N.; Prevot, M. S.; Sivula, K. *J. Phys. Chem. Lett.* **2014**, *5*, 3902−3908.
(28) Wang, P.; Minegishi, T.; Ma, G.; Takanabe, K.; Satou, Y.; Maekawa, S.; Kobori, Y.; Kubota, J.; Domen, K. *J. Am. Chem. Soc.* **2012**, *134*, 2469−2472.
(29) Ma, G.; Minegishi, T.; Yokoyama, D.; Kubota, J.; Domen, K. *Chem. Phys. Lett.* **2011**, *501*, 619−622.
(30) Wen, X.; Luo, W.; Zou, Z. *J. Mater. Chem. A* **2013**, *1*, 15479−15485.
(31) Li, B.; Yin, P.; Zhou, Y.; Gao, Z.; Ling, T.; Du, X. *RSC Adv.* **2015**, *5*, 2543−2549.
(32) Guan, Z.; Luo, W.; Zou, Z. *CrystEngComm* **2014**, *16*, 2929−2936.
(33) Riha, S. C.; Fredrick, S. J.; Sambur, J. B.; Liu, Y.; Prieto, A. L.; Parkinson, B. A. *ACS Appl. Mater. Interfaces* **2011**, *3*, 58−66.
(34) Ha, E.; Lee; Lee, Y. S.; Wang, J.; Li, F.; Wong, K. Y.; Tsang, S. C. E. *Adv. Mater.* **2014**, *26*, 3496−3500.
(35) Yu, X.; Shavel, A.; An, X.; Luo, Z.; Ibanez, M.; Cabot, A. *J. Am. Chem. Soc.* **2014**, *136*, 9236−9239.
(36) Seger, B.; Pedersen, T.; Laursen, A. B.; Vesborg, P. C. K.; Hansen, O.; Chorkendorff, I. *J. Am. Chem. Soc.* **2013**, *135*, 1057−1064.
(37) Kim, J.; Hiroi, H.; Todorov, T. K.; Gunawan, O.; Kuwahara, M.; Gokmen, T.; Nair, D.; Hopstaken, M.; Shin, B.; Lee, Y. S.; Wang, W.; Sugimoto, H.; Mitzi, D. B. *Adv. Mater.* **2014**, *26*, 7427−7431.
(38) Li, Z.; Luo, W.; Zhang, M.; Feng, J.; Zou, Z. *Energy Environ. Sci.* **2013**, *6*, 347−370.
(39) Kim, T. W.; Choi, K.-S. *Science* **2014**, *343*, 990−994.
(40) Jaime-Acuña, O. E.; Villavicencio, H.; Díaz-Hernández, J. A.; Petranovskii, V.; Herrera, M.; Raymond-Herrera, O. *Chem. Mater.* **2014**, *26*, 6152−6159.

DOI: 10.1021/jacs.5b09015
J. Am. Chem. Soc. 2015, 137, 13691−13697

(41) Chen, X.; Shen, S.; Guo, L.; Mao, S. S. *Chem. Rev.* **2010**, *110*, 6503−6570.
(42) Ohtani, B.; Pal, B.; Ikeda, S. *Catal. Surv. Asia* **2003**, *7*, 165−176.

DOI: 10.1021/jacs.5b09015
J. Am. Chem. Soc. 2015, 137, 13691−13697